Dispersion of spoof surface plasmons in open-ended metallic hole arrays

E. K. Stone* and E. Hendry†
School of Physics, University of Exeter, Stocker Road, Exeter EX4 4QL, United Kingdom
(Received 20 April 2011; published 22 July 2011)

Using phase sensitive microwave frequency measurements, we obtain the dispersion of spoof surface plasmon waves on a highly conducting sheet perforated with a two-dimensional array of subwavelength holes, and compare our results to an explicit analytical dispersion relation obtained by the modal matching method. We observe splitting into symmetric and antisymmetric surface modes, a behavior analogous to that of surface plasmons in thin metallic films at optical frequencies. We show that spoof surface modes play an important role in both near and far field transmissions. Specifically, we show that superfocussing effects which are present for surface plasmons in metallic films are absent for hole arrays (i.e., no amplification of near fields is possible for spoof surface plasmons). While many of the apparent properties of spoof surface plasmons resemble those of surface plasmons in thin metallic films, the analogy is therefore incomplete in the high frequency limit.

DOI: 10.1103/PhysRevB.84.035418 PACS number(s): 41.20.Jb, 84.40.−x, 42.30.Wb, 42.25.Bs

I. INTRODUCTION

Surface plasmons are electromagnetic modes with fields localized near the surface of a metal. The electromagnetic interaction between light and the metal is driven by the free electrons of the metal, which give rise to a negative permittivity for frequencies below their plasma frequencies. As a consequence, metals only support bound surface plasmons at frequencies near the plasma frequency of the metal. Surface plasmons are responsible for a host of interesting phenomena unique to metals.[1] For example, surface plasmons are thought to play an important role in the surface-enhanced Raman effect and anomalous transmission through subwavelength hole arrays in metal films.[2] More recently, Pendry[3] and others[4–6] highlighted the critical role that surface plasmons play in metal slab superlenses.

Bound surface plasmons in metal films are not supported at frequencies far from the metal plasma frequency. However, it has been shown that one can mimic the behavior of surface plasmons by structuring the surface of the conductor; for example, by introducing periodic arrays of dimples on the surface. Such a structured surface of a highly conducting sample can support surface plasmon-like modes at frequencies well below the plasma frequency of the conductor.[7–9] These surface modes have since become known as "designer" or "spoof" surface plasmon modes, with almost arbitrary dispersion generated through structure rather than material composition. For dimpled metal surfaces, the properties of spoof surface modes were first considered using simple analytical formalisms,[7–9] and have since been confirmed by rigorous numerical modeling[10–13] and experiments at microwave[14,15] and, subsequently THz frequencies.[16] Previous experimental work has found the dispersion of surface waves on open ended hole arrays at 337 μm (Ref. 17), but it should be noted that the curvature away from the lightline is due only to diffraction effects therefore only occurs close to the Brillouin zone boundaries.

In this paper, we investigate surface modes in two-dimensional arrays of subwavelength, open holes in a highly conducting sheet [shown in Fig. 1(a)]. It is thought that spoof plasmons might play an important role in the anomalous transmission displayed by such structures.[18–20] We employ phase-resolved, microwave-frequency measurements to obtain the dispersion of spoof surface plasmon waves, comparing our experimental results to dispersion relations obtained using a modified modal matching method, similar to that developed for dimpled conducting surfaces.[9] We observe splitting into symmetric and antisymmetric surface modes, a behavior analogous to that of surface plasmons in thin metallic films at optical frequencies. However, by considering the role of these spoof plasmon modes in near and far field transmission of our hole arrays, we show that the analogy breaks down in the high frequency limit, with superfocusing effects absent from hole array structures.

II. THEORETICAL FORMALISM

A. Modal matching approach

To better understand the properties of surface modes in open ended hole arrays, we start by introducing a rigorous modal matching model. Subwavelength hole arrays in metals at low frequencies (such as the THz range and below) have previously been modeled using modal-matching techniques.[21,22] We describe in brief how this technique works: the electromagnetic fields in the superstrate (assumed here to be air) and substrate are matched to the fields of the waveguide modes inside the subwavelength holes. By exploiting continuity of electric and magnetic fields at the boundaries, we can obtain explicit analytical expressions for transmission and reflection of a square array (period d) of square holes (side a) in a thin metallic sheet of thickness h. Below, we develop the formalism for this based on earlier work.[9,22]

We begin by defining expressions for the electric and magnetic fields in three regions of a hole array: in the incident vacuum region (superstrate), inside the holes, and in the substrate. For simplicity, note that in the following we omit the time (t) dependent component to the fields, $\approx \exp(i\omega t)$, where ω is the radial frequency. We consider a unit source field incident as shown in Fig. 1(a). We express the electric field on the incident side of the hole array (region 1) as a sum of our unit plane wave with wave vector, k_x, k_y, k_z, and a two-dimensional Fourier-Floquet expansion of diffracted orders with wave vectors, $k_x^{m_1,m_2}, k_y^{m_1,m_2}, k_z^{m_1,m_2}$. Approximating the

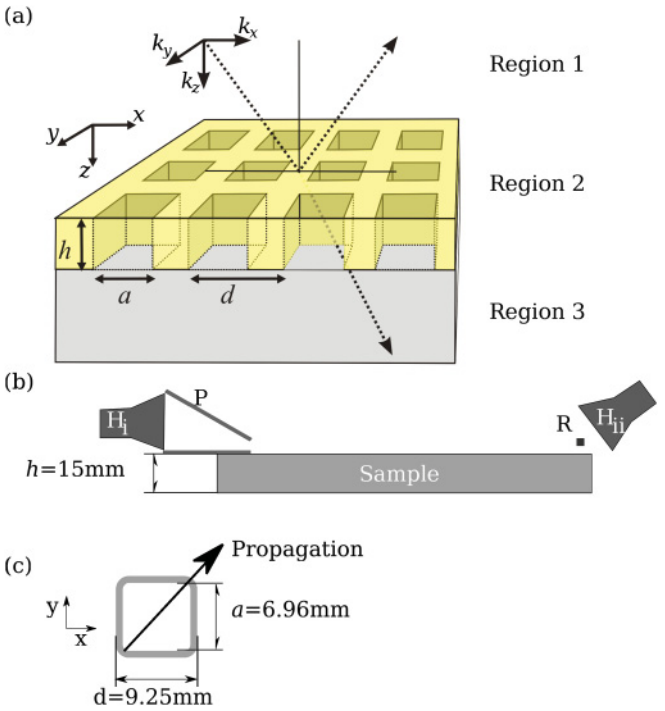

FIG. 1. (Color online) (a) Two-dimensional periodic array of square holes in a perfect conductor. The holes considered here are of depth h, side a, separated by distance d, and filled by dielectric material with ϵ_h, while the substrate (region 3) is defined by material with dielectric constant ϵ_{sub}. (b) A schematic side view of the experiment: a microwave horn H_{i} is directed into a wedge waveguide P. A second horn H_{ii}, is directed at a metal rod, R, $\approx$3 mm above the sample, which scatters power from the surface. (c) The unit cell of the sample used in the experiments. The arrow indicates the direction of propagation measured in the experiments.

metal as perfectly conducting (a reasonable approximation at THz and microwave frequencies), the electric field inside the holes (region 2) is expressed by the fundamental modes of a square cavity of width a, while in the substrate (region 3) we have again a Fourier-Floquet expansion of diffracted orders. These definitions amount to x components of the form

$$E_x^1 = \exp\left(ik_x x + ik_y y + ik_z^{0,0} z\right) + \sum_{m_1,m_2} r^{m_1,m_2}\psi_1^{m_1,m_2}\exp\left(-ik_z^{m_1,m_2} z\right), \quad (1a)$$

$$E_x^2 = \sum_{s_1,s_2} B^{s_1,s_2}\psi_2^{s_1,s_2}\exp\left(iq_z^{s_1,s_2} z\right) - C^{s_1,s_2}\psi_2^{s_1,s_2}\exp\left(-iq_z^{s_1,s_2} z\right), \quad (1b)$$

$$E_x^3 = \sum_{n_1,n_2} t^{n_1,n_2}\psi_1^{n_1,n_2}\exp\left[ik_z^{n_1,n_2}(z-h)\right], \quad (1c)$$

where $\psi_1^{m_1,m_2} = \exp[i(k_x + \frac{2m_1\pi}{d})x]\exp[i(k_y + \frac{2m_2\pi}{d})y]$ and $\psi_2^{s_1,s_2} = \sin(\frac{s_1\pi}{a}y)\cos(\frac{s_2\pi}{a}x)$. Note that similar expressions for y components of field can also be defined. The integer pairs (m_1,m_2) and (n_1,n_2) denote the diffracted orders, on the incident and substrate sides of the hole array, respectively, from the grating of pitch d. The factors r^{m_1,m_2} and t^{n_1,n_2} describe the field reflection and transmission coefficients. The z component of the incident and transmitted wave vectors can be written as

$$k_z^{m_1,m_2} = \sqrt{k_0^2 + \left(k_x + \frac{2m_1\pi}{d}\right)^2 + \left(k_y + \frac{2m_2\pi}{d}\right)^2}, \quad (2a)$$

$$k_z^{n_1,n_2} = \sqrt{\epsilon_{\text{sub}}k_0^2 + \left(k_x + \frac{2m_1\pi}{d}\right)^2 + \left(k_y + \frac{2m_2\pi}{d}\right)^2}, \quad (2b)$$

where c is the speed of light, $k_0 = \omega/c$ is the wave number of the incident light and ϵ_{sub} is the dielectric constant of the substrate material (region 3). The factors B^{s_1,s_2} and C^{s_1,s_2} describe the electric field amplitudes of the decaying wave in the cavity and the reflected wave from the cavity bottom, respectively, where the integer pair (s_1,s_2) define the waveguide mode within the cavity. Though we explicitly develop our formalism here based around square holes, it is relatively straightforward to consider other waveguide shapes with different explicit forms of $\psi_2^{s_1,s_2}$. For square holes, the propagation constant in the cavity is

$$q_z^{s_1,s_2} = \sqrt{\epsilon_h k_0^2 - \left(\frac{s_1\pi}{a}\right)^2 - \left(\frac{s_2\pi}{a}\right)^2}, \quad (3)$$

where ϵ_h is the dielectric constant of the material inside the cavity.

We can obtain the z components of the electric field in the three regions of space, and subsequently expressions for the magnetic field $\mathbf{H}$, through the free space Maxwell's relations $\nabla\cdot\ \mathbf{E} = \mathbf{0}$ and $\nabla\times\mathbf{E} = -\mu_0\delta\mathbf{H}/\delta t$. This gives the x and y components of the electric and magnetic fields in all regions in terms of the set of unknowns r,t,B, and C. To eliminate some of the these unknowns, we can use the fact that both the x and y components of the electric field must be continuous at the vacuum-sample interfaces (i.e., $z = 0$ and $z = h$, where h is the depth of the hole array) over the entire unit cell, while the magnetic field components are continuous only at the hole aperture. Matching the E fields in regions 1 and 2 at $z = 0$, and in regions 2 and 3 at $z = h$, (i.e., multiplying by ψ_1^* and integrating over x and y from 0 to d), and taking into account the orthogonality of the eigenmodes of the system, yields sets of continuity equations of the form

$$(\delta^{m_1,m_2} + r^{m_1,m_2})d^2 = \sum_{s_1,s_2}(B^{s_1,s_2} - C^{s_1,s_2})Q_1^{m_1,m_2,s_1,s_2}, \quad (4a)$$

$$t^{n_1,n_2}d^2 = \sum_{s_1,s_2}\left(B^{s_1,s_2}e^{iq_z^{s_1,s_2}h} - C^{s_1,s_2}e^{-iq_z^{s_1,s_2}h}\right)Q_1^{n_1,n_2,s_1,s_2}, \quad (4b)$$

where

$$Q_1^{m_1,m_2,s_1,s_2} = \int_0^a \sin\left(\frac{s_1\pi y}{d}\right)\cos\left(\frac{s_2\pi x}{d}\right) \times \exp\left[-i\left(k_x + \frac{2m_1\pi}{d}\right)x\right] \times \exp\left[-i\left(k_y + \frac{2m_2\pi}{d}\right)y\right]dxdy, \quad (4c)$$

is the overlap integral between the diffracted order (m_1,m_2) and the waveguide mode (s_1,s_2) and δ^{m_1,m_2} represents the Kronecker delta function $\delta(m_1)\delta(m_2)$. We also obtain separate expressions for the continuity of the y components of electric field.

We can obtain a further set of equations by considering the continuity of the H field over the holes at $z = 0$ and $z = h$, respectively, that is, by multiplying H by ψ_2, and integrating from 0 to a for x and y. This gives a set of equations containing a second overlap integral

$$Q_2^{m_1,m_2,s_1,s_2} = \int_0^a \sin\left(\frac{s_1\pi y}{d}\right)\cos\left(\frac{s_2\pi x}{d}\right) \times \exp\left[+i\left(k_x+\frac{2m_1\pi}{d}\right)x\right] \times \exp\left[+i\left(k_y+\frac{2m_2\pi}{d}\right)y\right]dxdy. \quad (4d)$$

These equations, relating the x and y components of the electric and magnetic fields, define a complete set of equations describing the components of the fields in terms of the unknown sets r^{m_1,m_2},t^{n_1,n_2},B^{s_1,s_2}, and C^{s_1,s_2}. The number of equations present in the set depends on the number of diffracted orders and waveguide modes we include in the calculation, but the system of equations is always uniquely defined (i.e., the number of unknowns equals the number of equations). For a rigorous solution to the system of equations, we must include a high number of diffraction orders and waveguide modes. It is then straightforward, if rather laborious, to solve the continuity equations, eliminating the coefficients B^{s_1,s_2} and C^{s_1,s_2}, to obtain the complex reflection and transmission coefficients, r^{m_1,m_2} and t^{n_1,n_2}.

B. Dispersion relations

To satisfactorily separate the diffraction effects (photonic band gap) from the dispersion of a spoof plasmon, it is necessary to study effects far from the Brillouin zone boundary at $k_x = \pi/d$. In our experiments (see below) this is achieved by studying surface modes in the (1,1) direction of the unit cell. We therefore derive the dispersion relations of the surface modes propagating in this direction (i.e., with $k_x = k_y$ and $E_x = E_y$) and restrict ourselves for now in discussing the dispersion when both regions 1 and 3 are air (i.e., $\epsilon_{\text{sub}} = 1$). For such circumstances, the Fourier components of the fields in regions 1 and 3 have components of mode wave vector in the z direction which can be written as

$$k_z^{m_1,m_2} = \sqrt{k_0^2 + \left(\frac{k_\parallel}{\sqrt{2}}+\frac{2m_1\pi}{d}\right)^2 + \left(\frac{k_\parallel}{\sqrt{2}}+\frac{2m_2\pi}{d}\right)^2}, \quad (5)$$

where $k_\parallel$ is the component of the wave vector parallel to the surface.

Even while restricting ourselves to surface modes in the (1,1) direction, a solution including large numbers of diffracted orders and waveguide modes must be found numerically. However, there are a number of simplifications commonly applied in modal matching which can drastically reduce the complexity of the problem and make an analytical solution possible. We first introduce these simplifications and then discuss their validity below. As the simplest solution, we can limit ourselves to considering only the first order waveguide mode ($s_1 = 1,s_2 = 0$) in the cavity and specular reflection/transmission ($m_1 = m_2 = n_1 = n_2 = 0$). This is the approximation used in Refs. 7 and 8 by Pendry *et al.* to drive analytical dispersion relations for spoof surface plasmons on dimpled conducting surfaces. The approximation is valid only in the limit $a \ll d \ll \lambda_0$, where λ_0 is the vacuum wavelength. Then, the summations in Eqs. (4a), (4b), and those in the continuity equations for magnetic fields, are removed, and one can easily solve the continuity equations, eliminating the coefficients $B^{1,0}$ and $C^{1,0}$. The transmission coefficient found is

$$t^{0,0} = -\frac{2q_z^{1,0}k_0^2}{k_z}\frac{a^2}{d^2}\frac{Q_1^{0,0,1,0}Q_2^{0,0,1,0}}{\exp\left(iq_z^{1,0}h\right)\left(F-\frac{a^2q_z^{1,0}}{2}\right)^2 - \exp\left(-iq_z^{1,0}h\right)\left(F+\frac{a^2q_z^{1,0}}{2}\right)^2}, \quad (6a)$$

where

$$F = \frac{Q_1^{0,0,1,0}Q_2^{0,0,1,0}}{d^2}\left(\frac{k_0^2}{k_z^{0,0}}\right). \quad (6b)$$

From this solution, one can also infer the dispersion of surface modes, given by the poles in transmission

$$\exp\left(iq_z^{1,0}h\right)\left(F-\frac{a^2q_z^{1,0}}{2}\right)^2 - \exp\left(-iq_z^{1,0}h\right)\left(F+\frac{a^2q_z^{1,0}}{2}\right)^2 = 0. \quad (6c)$$

One should note that on increasing the depth of the holes to infinity ($h \to \infty$) one recovers from Eq. (6c) the dispersion relation $F = \frac{a^2q_z^{1,0}}{2}$, precisely the dispersion relation found by Pendry *et al.* for spoof plasmons in arrays with infinitely deep, square holes.[7,8]

Near the cutoff frequency of the cavities, one can qualitatively argue that considering only the lowest order transverse electric (TE) waveguide mode (i.e., $s_1 = 1,s_2 = 0$) is a reasonable assumption: the higher order waveguide modes with the correct symmetry are very strongly evanescent [i.e., in Eq. (3), $q_z^{s,t}$ is large and imaginary] and will therefore have little effect on the surface mode dispersion. However, numerical (using finite element,[6] modal expansion,[7] and finite time domain)[8] and analytical (modal matching)[9] modeling has shown that the hole period can be particularly critical in determining the precise dispersion relation of the surface mode supported. This is because diffracted evanescent waves change the boundary conditions at the entrance and exit of the cavities. It has been shown for dimpled surfaces[9] that including higher diffraction orders while describing the fields inside the

cavities using only the first order waveguide mode provides an accurate dispersion relation. For the holey metal layers discussed here, this approximation gives the transmission coefficient

$$t^{m_1,m_2} = -\frac{2q_z^{1,0}k_0^2}{k_z}\frac{a^2}{d^2}\frac{Q_1^{m_1,m_2,1,0}Q_2^{0,0,1,0}}{\exp\left(iq_z^{1,0}h\right)\left(\sum_{m_1,m_2}F^{m_1,m_2}-\frac{a^2q_z^{1,0}}{2}\right)^2-\exp\left(-iq_z^{1,0}h\right)\left(\sum_{m_1,m_2}F^{m_1,m_2}+\frac{a^2q_z^{1,0}}{2}\right)^2}, \tag{7a}$$

$$F^{m_1,m_2} = \frac{Q_1^{m_1,m_2,1,0}Q_2^{m_1,m_2,1,0}}{d^2}\left(\frac{k_0^2+\left(\frac{k_\parallel}{\sqrt{2}}+\frac{2m_1\pi}{d}\right)\left(\frac{2m_2\pi}{d}-\frac{2m_1\pi}{d}\right)}{k_z^{m_1,m_2}}\right), \tag{7b}$$

with surface mode dispersion given by

$$\exp\left(iq_z^{1,0}h\right)\left(\sum_{m_1,m_2}F^{m_1,m_2}-\frac{a^2q_z^{1,0}}{2}\right)^2 - \exp\left(-iq_z^{1,0}h\right)\left(\sum_{m_1,m_2}F^{m_1,m_2}+\frac{a^2q_z^{1,0}}{2}\right)^2 = 0. \tag{7c}$$

The summations over the integer diffracted orders are typically carried out for $m_1 = -1,0,+1$ and $m_2 = -1,0,+1$ as in Ref. 9.

One should note that the modal matching solutions presented above are only strictly valid for frequencies well below the cutoff frequency of the second order waveguide mode.

III. RESULTS AND DISCUSSION

A. Measurement of surface mode dispersion

To validate the dispersion relations derived in the previous section, we have measured the surface modes supported by open hole array structures in the microwave frequency region. We use a close packed array of hollow, square-ended brass tubes, with side length $d = 9.25$ mm, inner length $a = 6.96$ mm and height $h = 15$ mm. The cutoff frequency of the holes is defined as $\omega_{co} = \frac{\pi c}{a\sqrt{\epsilon_h}}$, where ϵ_h is the dielectric constant of the material inside the tubes. As we are interested in observing the surface modes unperturbed by effects due to the Brillouin zone boundary, we require ω_{co} to be far below the diffraction edge associated with the sample: in this case the diffraction edge in the (1,0) direction occurs at 17.7 GHz. To first minimize the effects of the proximity of the Brillouin zone boundary the holes are filled with dielectric material ($\epsilon_h = 2.29$), giving a cutoff frequency of 14.4 GHz for the cavities in our sample. Since this is close to the (1,0) diffraction edge of our sample, one would expect the dispersion of surface modes in the (1,0) direction to be strongly perturbed by the band gap at the Brillouin zone boundary. In experiment, we therefore measure in the diagonal of the unit cell (i.e., $k_y = k_x$): the diffraction edge in the (1,1) direction is 22.3 GHz, significantly greater than the cutoff frequency of our holes, thereby reducing the perturbation due to diffraction. This perturbation is discussed in more depth in Sec. III B. Note that due to the presence of open ended holes, the arrays considered here exhibit very different electromagnetic behavior from the structures considered in Refs. 9 and 15.

There are several methods by which one can investigate the dispersion of surface modes. The so-called "prism coupling" can be used, in which one uses the evanescent fields associated with the total internal reflection at a high dielectric boundary to couple to a surface wave, such as in the Kretchman configuration.[15,23] However, such techniques usually allow for coupling only to antisymmetric surface waves (i.e., modes where the fields do not exhibit mirror symmetry in the plane of the sample). Coupling to a surface mode via a grating is also possible,[24,25] but typically leads to significant distortion of the dispersion. To avoid these drawbacks, we have developed an alternative method: Fig. 1(b) shows the experimental setup used. In brief, we use a vector network analyzer (VNA)[26] which operates in the microwave frequency range using broadband coupling horns (10–50 GHz). At "i" in Fig. 1(b) a horn is directed into a wedge waveguide with a 5-mm exit aperture. At "ii," a horn is directed toward a long thin metallic rod positioned 3 mm above the sample surface. The height of this rod can be varied to modify the coupling efficiency to each of the surface modes of the sample.

The dispersion is obtained from phase measurements of a propagating surface wave. The difference in phase between two surface waves at a point in space ($\Delta\phi$) is related to the difference in the in-plane wave vector component ($\Delta k_\parallel$) through the simple relation

$$\Delta k_\parallel = \frac{\Delta\phi}{L}, \tag{8}$$

where L is the propagation length from the source. In our experiments, we use a propagation length of 30 cm. To obtain the absolute magnitude of the in-plane wave vector component, one needs a reference measurement. We therefore compare the phase of the wave measured across our sample to that of a planar metal sheet (which we assume to possess a surface mode propagating at the speed of light in vacuum). Taking the phase difference between these two measurements and dividing by the propagation length gives $\Delta k_\parallel$ with respect to a free space wave, represented by the light line in Figs. 2 through 4, and therefore yields a dispersion curve. The dispersion curves for our open ended hole array (i.e., $\epsilon_{sub} = 1$) are shown in Fig. 2. The circles are extracted from the measured phase information as described above. We clearly observe two surface modes in the frequency range of interest. However, one should note that the measured dispersion for the higher frequency surface mode (triangles) is obtained in a nonrigorous manner, by assuming

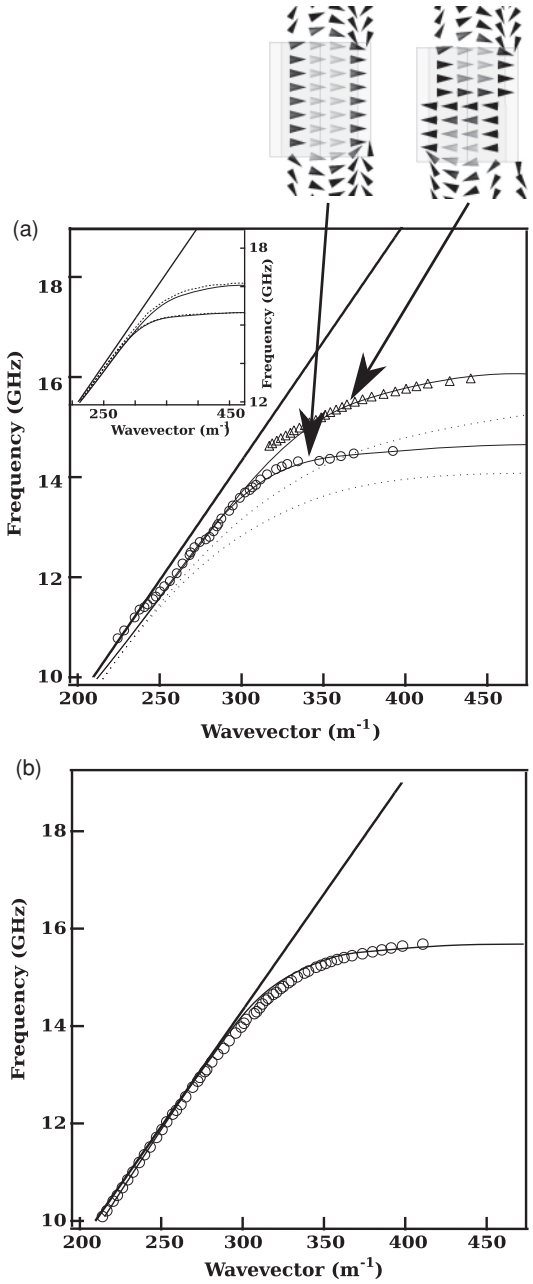

FIG. 2. Experimentally determined spoof surface plasmon dispersion curves (circles and triangles) compared to the analytical models (doted curved lines), for an array defined by $d = 9.25$ mm, $a = 6.96$ mm, $h = 15$ mm, $\epsilon_h = 2.29$). (a) For an open ended hole array (i.e., $\epsilon_{\text{sub}} = 1$), one observes both low frequency (symmetric) and higher frequency (antisymmetric) modes. The arrows indicate the electric field profiles calculated using the finite element method (FEM) (Ref. 27). These show the direction of the electric fields inside the hole for a particular phase (with the lighter color indicating a strong electric field) highlighting the symmetric and antisymmetric nature of the two surface modes. The dotted line in this figure shows the analytical results for both modes when diffracted orders are not taken into account. (b) For a dimpled surface array (i.e., $\epsilon_{\text{sub}} = i\infty$) we observe only one surface mode, with an asymptomatic frequency higher than the cutoff frequency of the holes (see text). In both (a) and (b) the straight solid line represents the vacuum light line. Inset of (a): comparison between analytical and numerical (FEM) (Ref. 27) models.

the onset of this mode occurs at the lightline for frequencies above the asymptotic frequency of the lower frequency mode. Despite this assumption, both of these modes exhibit good agreement with the analytical model from Eq. (7c) (solid curved lines).

We have also conducted full numerical finite element method (FEM) modeling of the surface eigenmodes carried by our sample.[27] The numerical modeling predicts surface mode dispersions which correlate extremely closely to those from our simple analytical model derived above [FEM modeling is shown as the dashed line in the inset of Fig. 2(a), while the analytical model is represented by the solid line]. We can also obtain distributions associated with each surface mode: the boxes above Fig. 2(a) show the electric fields inside the hole region, with the direction of the electric field represented at the same point in phase cycle. These show the low frequency mode as having a symmetric electric field distribution while the higher frequency mode has an antisymmetric distribution.

The splitting of the surface mode into symmetric and antisymmetric modes is very reminiscent of the behavior of surface plasmons in thin metallic films at optical frequencies.[28] However, such splitting is not observed for the surface modes on dimpled surfaces (i.e., with closed holes, where region 3 is a perfect metal with $\epsilon_{\text{sub}} = i\infty$) considered in Refs. 8,9,12,14–16. The dispersion of the spoof plasmon measured on a dimpled surface with the same dimension as our hole array is shown in Fig. 2(b). Our measurements are compared to the analytical modal matching solution for a dimpled surface from Ref. 9. For both the measurement and the analytical model we observe only one spoof plasmon mode asymptotically diverging from the light line. This behavior arises due to the boundary conditions between regions 2 and 3, which, for closed holes, forces the transverse component of the electric field to zero at this interface. For open holes this restriction is lifted, and a node can appear in the middle of the holes ($z = \frac{h}{2}$): this is the defining feature of antisymmetric surface mode of the open hole arrays.

In addition to the mode splitting, which appears for the open holes and is absent from closed holes, there is a clear difference in the asymptotic frequencies of the dispersions for the two cases. We address this in the next section.

B. Asymptotic frequencies and mode splitting

For the simplest modal matching solution, that is, considering only *first order waveguide mode* ($s_1 = 1, s_2 = 0$) in the cavity and *specular reflection/transmission* ($m_1 = m_2 = n_1 = n_2 = 0$), one obtains the dispersion relation from Eq. (6c). From this simplified form of the dispersion relation, one can easily obtain the asymptotic frequencies for dispersion of the surface waves. The lowest frequency asymptote is given by the cutoff frequency of the holes, $\omega_{\text{co}} = \frac{\pi c}{a\sqrt{\epsilon_h}}$. It should be noted that, in contrast to the spoof surface plasmon of dimpled metal surfaces,[9] the asymptotic frequency of the lowest frequency surface mode in these hole arrays is *independent of hole depth*. This behavior can be seen in the low frequency dispersion of a thicker hole array [$h = 40$ mm, solid curves in Fig. 3(a)], which displays the same asymptotic frequency as our sample

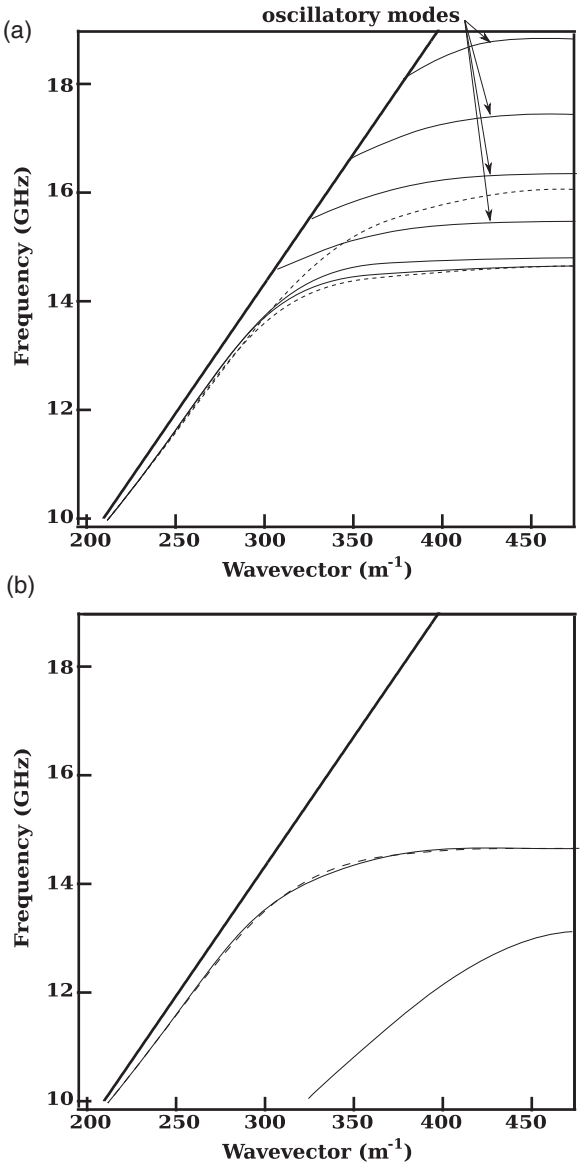

FIG. 3. (a) Surface mode dispersion for larger array thickness $h = 40$ mm. The asymptotic frequency of the symmetric mode remains relatively unchanged, while the asymptotic frequency of the antisymmetric mode has reduced in frequency. In addition, one observes the surface modes associated with the higher frequency waveguide modes, marked with arrows. (b) The effect of introducing a substrate (region 3) with nonunity dielectric constant, $\epsilon_{\text{sub}} = \epsilon_h = 2.29$ is to split the surface mode, with each mode following a different light line associated with the material on each interface. The dashed lines in both figures show the dispersion for the measured sample (defined by $d = 9.25$ mm, $a = 6.96$ mm, $h = 15$ mm, $\epsilon_h = 2.29$, and $\epsilon_{\text{sub}} = 1$).

[$h = 15$ mm, dashed curves in Fig. 3(a)]. However, for the higher order antisymmetric mode (as thickness increases) the asymptotic frequency decreases.

In addition to the two spoof surface plasmons, for structures with larger h [Fig. 3(a)] we observe several higher order modes which do not asymptote to the light line. Indeed, we actually have a complete family of surface modes with asymptotic frequencies derived from the condition $\tan(q_z^{1,0}h) = 0$, that is, with asymptotic frequencies, ω_{as}, given by

$$\omega_{as} = \omega_{\text{co}}, \sqrt{\omega_{\text{co}}^2 + \left(\frac{\pi c}{h\sqrt{\epsilon_h}}\right)^2}, \sqrt{\omega_{\text{co}}^2 + 2\left(\frac{\pi c}{h\sqrt{\epsilon_h}}\right)^2}, \ldots . \tag{9}$$

Since $k_x > k_0$, all modes exhibit fields which are evanescent in regions 1 and 3, above and below the hole array, and so can be termed surface modes. However, the fields inside the holes distinguish each of the modes: the lowest frequency mode, defined by the asymptote at the cutoff frequency of the holes, exhibits electric fields inside the hole which are hyperbolic and symmetric in form (though not explicitly shown here, it is straight forward to solve the continuity equations for the factors B and C which determine the electric field profiles). The second lowest frequency mode, with an asymptotic frequency at $\sqrt{\omega_{\text{co}}^2 + (\frac{\pi c}{h\sqrt{\epsilon_h}})^2}$, exhibits a node in the electric field in the middle of the hole [see inset of Fig. 2(a)]. The fields of this mode are hyperbolic and *antisymmetric* in form for frequencies below ω_{co}. These two lowest order modes are reminiscent of the symmetric and antisymmetric surface plasmons in thin metal films,[28] and are therefore labeled here as the "spoof plasmon" modes of the hole array. Similar to the behavior of symmetric and antisymmetric surface plasmons, both the symmetric and antisymmetric spoof plasmon modes are asymptotic to the light line.

The fields inside the hole for the higher order modes are oscillatory in nature (labelled "oscillatory modes" here), with field maxima at the hole entrance and exit plus two or more nodes. The oscillatory fields inside the holes exist only in the frequency domain $\omega > \omega_{\text{co}}$, and are therefore not asymptotic to the light line. When the depth of the holes is increased [Fig. 3(a)] one observes a reduction in the asymptotic frequencies of these modes. For infinitely deep holes, the asymptotic frequencies of these modes converge onto that of the symmetric spoof surface plasmon mode.

We have discussed above the surface mode dispersion in its very simplest form, by considering only specular reflection and transmission. However, numerical (using finite element,[6] modal expansion,[7] and finite time domain)[8] and analytical (modal matching)[9] modeling has shown that diffracted evanescent waves can be crucial to obtain an accurate dispersion relation.[9] In Fig. 2(a) we compare the measured dispersion (points) to the dispersion relations from Eqs. (6c) and (7c) (excluding and including evanescent diffracted orders, respectively). One can clearly see the important role that evanescent diffracted fields play in determining surface mode dispersion. These higher order Fourier components to the electromagnetic fields not only perturb the frequency dependence of the dispersion, but also lead to slightly higher asymptotic frequencies than predicted by Eq. (9). This behavior has previously been observed for spoof surface plasmons on dimpled metal surfaces,[9] and is related to a modification by the evanescent diffracted fields of the boundary conditions at the entrance and exit of the cavities (which, in turn, perturbs the quantization of the field inside the holes).

In addition to the diffracted fields, surface mode dispersion is also perturbed by the presence of a substrate. In Fig. 3(b),

the dispersion for a structure with a dielectric substrate ($\epsilon_{sub} = \epsilon_h = 2.29$ in region 3) is shown as a solid line. The presence of a substrate results in a further splitting of the symmetric and antisymmetric spoof surface plasmons. The lower frequency mode asymptotes to the light line in a material of ϵ_{sub}, while the higher frequency mode asymptotes to the vacuum light line. This behavior is again reminiscent of surface plasmons in thin metallic films on a dielectric substrate.[28]

IV. ROLE OF SURFACE MODES IN HOLE ARRAY TRANSMISSION

A. Near field transmission

Discovered originally by Pendry,[3] an interesting property of surface plasmons is their ability to focus light to spots smaller than the diffraction limit for light, an effect referred to as superlensing. The simplest form of a superlens consists of a simple metallic film which exhibits superlensing effects near the surface plasmon resonance condition in the near ultraviolet frequency region.[4–6] At this frequency a near field source of radiation couples to the symmetric surface plasmon of a thin metal film. An important question to answer is therefore: Can a symmetric spoof surface plasmon exhibit similar superlensing properties?

The electromagnetic fields scattered by an object may be represented by a Fourier sum. To form a perfect image from the field scattered by an object, one must restore all Fourier components of the field in an image plane. However, Fourier components associated with the large lateral wave vectors $k_\parallel$ satisfying $|k_\parallel| > |k_0|$ give rise to evanescent waves which have imaginary values for k_z. These near field components are confined to the subwavelength vicinity of the object. Hence, in a normal lens one can usually only capture wave vectors satisfying the condition $|k_{\text{parallel}}| < |k_0|$, limiting the resolution of image formation to approximately the wavelength of light. In the last decade it has, however, become clear that it is possible to design superlenses which can restore at least some of these near field components, allowing subwavelength resolution in images.[4] In this section, we consider the transmission of near fields of our hole arrays within our analytical formalism from Sec. II. We show below that spoof surface plasmons play an important role in determining the near field transmission characteristics of a hole array.

Ignoring the effects of diffraction for now, the field transmission function of interest is given by Eq. (6a). In general, the transmission function introduces some perturbations of the fields which are dependent on $k_\parallel$. However, for frequencies near the surface mode resonances given by Eq. (9), the conditions $e^{iq_z h} \approx 1$ and $e^{-iq_z h} \approx 0$ apply, and Eq. (6a) simplifies to $t^{0,0} \to 1$ for $k_\parallel \to \infty$. This means that, in the absence of diffraction, near fields defined by large lateral wave vectors will be perfectly transmitted through a hole array. This effect has recently been pointed out by Jung *et al.*,[29] who described hole array structures as "perfect endoscopes," that is, structures which are capable of perfectly transforming a source of field from the input to output surfaces without losses, while maintaining subwavelength resolution. This interesting property occurs for an array of *any* hole depth (i.e., input fields can be transferred to the output interface of a hole array over an arbitrarily large distance).

In practice, perfect transmission will not be achieved due to the effects of diffraction. Including diffracted orders, the relevant transmission is given by Eq. (7a). For frequencies near to ω_{co} (i.e., where the condition $q_z^{1,0} h \approx 0$ applies), Eq. (7a) simplifies to $t^{0,0} \approx F^{0,0}/\sum m_1,m_2 F^{m_1,m_2}$. This results in perfect transmission only for $|F^{0,0}| \gg |F^{m_1,m_2}|$ (i.e., when $|k_z^{0,0}| \ll |k_z^{m_1,m_2}|$). Hence, the Brillouin zone boundary sets a limit for transmission of evanescent fields to those with $|k_\parallel| < \frac{2\pi}{d}$ [see Eq. (5)]. This is in agreement with the numerical modeling of Jung *et al.*,[29] who found that resolution of their hole array endoscope is limited by the periodicity of the array.

However, it should be noted that a "perfect endoscope" is not the same as a "perfect lens".[3] For a plasmonic metal film at the surface plasmon frequency, it is straightforward to show that the thin film transmission $t \to \exp(-ik_z h)$ for $k_\parallel \to \infty$ (Ref. 3). Therefore, for evanescent field components with imaginary k_z, the fields are effectively amplified on transmission of the metallic film. This highlights one of the fundamental differences between a surface plasmon and a spoof surface plasmon: while surface plasmons in metallic films can give rise to lensing effects for evanescent fields, spoof surface plasmons in hole arrays *cannot* give rise to such effects. This difference is due to the nature of the fields inside the materials: at their asymptotic frequency, surface plasmons exhibit fields inside the metal which are evanescent in nature. At the asymptotic cutoff frequency of a symmetric spoof surface plasmon, meanwhile, the fields inside the cavities lose their evanescent character. Hence, no amplification of near fields is possible for spoof surface plasmons. Since spoof surface plasmons have very different near field characteristics to surface plasmons, the term "spoof surface plasmon" may be something of a misnomer. However, we note that superfocussing at microwave and THz frequencies may still be possible with semiconductor surface plasmons.[30]

B. Far field transmission

Recent interest in the enhanced optical transmission through arrays of subwavelength holes in metal films was sparked by the seminal work of Ebbesen *et al.*,[2] who observed peaks in transmission at wavelengths close to the lattice periodicity. Since this visible-frequency observation of enhanced optical transmission through hole arrays, similar effects have been observed at infrared,[31] Terahertz,[32–36] and microwave frequencies,[37,38] with applications suggested in designing filters,[39] optical sensors,[40] microwave devices,[41] and THz optical components.[42]

Since the first experimental observations, consensus has been gradually developing that surface modes (surface plasmons at optical frequencies) play a crucial role in enhanced optical transmission. In this respect, perhaps the most physically insightful model applied to hole arrays has been the "Fano-type" mechanism.[18,43] In this picture, transmission is interpreted in terms of the interference between two transmission channels: one nonresonant (direct) channel describes transmission through individual, uncoupled holes while the resonant channel describes light which transverses the grating through adjacent holes via diffractive coupling to surface

modes. Within this model, one can understand the origin of peaks in the transmission spectra of the hole arrays in terms of constructive interference conditions, reached when the wavelength of the light is approximately equal to the spacing of the hole-array lattice. In this section we highlight the role that spoof surface plasmons play in this process. The effects we discuss below are entirely scalable with wavelength and array size. We therefore choose to normalize all length scales by the period of the array d and normalize frequency and wave vector by the grating frequency and vector, respectively,

$$\omega_{\text{diff}} = \frac{2\pi c}{d}, \quad k_{\text{diff}} = \frac{2\pi}{d}. \tag{10}$$

For simplicity, we restrict ourselves to the discussion of surface waves propagating in the (1,0) direction of the unit cell. We note that the evanescent surface modes, which strictly exist only in the region described by $k_x > k_0$, do not contribute to transmission in the far field. However, the influence of surface modes in the region $k_x < k_0$ can be considered by employing a reduced zone representation of surface modes. Briefly, one finds the surface mode dispersions without any diffraction effects. Then, periodicity is introduced by adding and subtracting grating vector components of magnitude k_{diff} through $k'_x = k_x \pm m_1 k_{\text{diff}} \pm m_2 k_{\text{diff}}$. A similar approach is commonly employed to analyze the effects of surface plasmons in optical gratings.[44] Note that we neglect the opening of band gaps near the Brillouin zone boundary, and so this approach should only be treated as approximate. In Figs. 4(a) and (b), black lines represent mode wave vectors, k_x, in the absence of diffraction [from Eq. (6c)], while grey dashed lines represent k'_x under first order diffraction (i.e., $m_1 = 1, m_2 = 0$). In this reduced zone representation, for hole arrays defined by $\omega_{\text{co}} < \omega_{\text{diff}}$ [Fig. 4(a)], a number of modes appear in the region $k_x < k_0$. One can therefore expect multimodal features in transmission. The two lowest frequency transmission features arise from diffractive coupling to the spoof plasmon surface modes, while the higher frequency features arise from coupling to the oscillatory modes of the cavity. Transmission spectra of these large hole structures can therefore be very complex, since one can expect many peaks associated with each diffraction order. For hole arrays with $\omega_{\text{co}} > \omega_{\text{diff}}$ (Fig. 4), one observes only the two lowest frequency modes below ω_{diff}. This is because only symmetric and antisymmetric surface plasmon modes are asymptotic to the light line (as discussed in Sec. III B). For such a structure one expects bimodal features in transmission.

Multimodal and bimodal behavior can be observed in Figs. 4(c) and (d), respectively. The transmission, calculated using Eq. (7a) is plotted as a function of hole height h for a large hole array with $a = 0{,}8d$, and a small hole array with $a = 0.4d$. For the array with large holes, the transmission typically contains several convoluted peaks, each associated with diffractive coupling to a different surface mode. As h decreases, higher order modes extend toward the light line and converge at $\omega/\omega_{\text{diff}} = 1$. The transmission resonances associated with these modes can become very narrow as dephasing decreases.[18] For the array with small holes, on the other hand, transmission is mediated only by diffractive

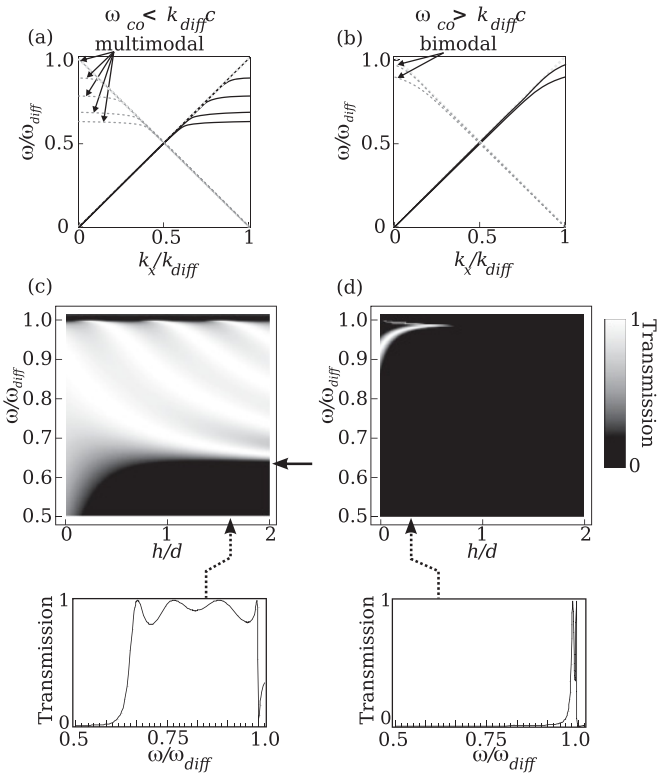

FIG. 4. (a) Spoof surface mode dispersion relations in the reduced zone representation. For hole arrays defined by $\omega_{\text{co}} < \omega_{\text{diff}}$, a number of modes associated with each grating vector are observable in the first Brillouin zone. For hole arrays with $\omega_{\text{co}} > \omega_{\text{diff}}$ (b) only the first two (surface plasmon) modes are defined below cutoff. (c) Transmission as a function of hole height h for an array with dimensions $a = 0.8d$. One can clearly observe the multimodal transmission, with several peaks in the frequency region between the cut-off frequency (marked by a solid arrow) and $\omega = \omega_{\text{diff}}$. (d) Transmission as a function of hole height h for an array with dimensions $a = 0.4d$, showing the transmission mediated by the symmetric and antisymmetric surface plasmon modes. The lower panels show transmission spectra at heights indicated by dotted arrows. All calculations are for $\epsilon_h = 1$.

coupling to the symmetric and antisymmetric surface plasmon modes. By tuning the hole size so that ω_{co} lies above or below ω_{diff}, one can therefore easily change from bimodal to multimodal transmission regimes. This behavior illustrates why hole array structures make excellent tunable filters, as they can be specifically designed as either narrowband or broadband transmission filters with a relatively small change to structural dimensions.

V. CONCLUSION

Phase sensitive microwave experiments have been conducted to measure the dispersion of surface modes for a structure consisting of an array of holes in a highly conducting sheet. Two separate surface modes were observed and shown to have field distributions analogous to the symmetric and antisymmetric surface plasmon modes found in thin metal films. To analyze our measurements, we have developed explicit analytical expressions for the transmission function of our hole arrays using a modal matching method. The

dispersion relations found from this approach have shown very close agreement to the measurements. Using our analytical functions, we show that spoof surface modes play an important role in enhanced optical transmission, and elucidate the hole and depth behavior in the transmission of such structures. In the near field transmission, we discuss the role these surface modes play in endoscopic transmission (the transfer of a field profile from the incident to output interfaces), and show that the theoretical limit for near field spatial resolution is the period of the hole array. However, we show that superfocussing effects which are present for surface plasmons in metallic films are absent for hole arrays (i.e., no amplification of near fields is possible for spoof surface plasmons). While many of the apparent properties of spoof surface plasmons resemble those of surface plasmons in thin metallic films, the analogy breaks down in the high frequency limit.

ACKNOWLEDGMENTS

This work was supported through funding from the RCUK and EPSRC. The authors also wish to thank Melita Taylor, Alastair Hibbins, Tom Isaac, Ian Hooper, and Stavroula Fontonopolu for helpful discussions, and Elizabeth Brock and Helen Rance for assisting with the experiments.

*e.k.stone@exeter.ac.uk
†e.hendry@exeter.ac.uk

[1] W. L. Barnes, A. Dereux, and T. W. Ebbesen, Nature (London) **424**, 824 (2003).
[2] T. W. Ebbesen, H. J. Lezec, H. F. Ghaemi, T. Thio, and P. A. Wolff, Nature (London) **391**, 667 (1998).
[3] J. B. Pendry, Phys. Rev. Lett. **85**, 3966 (2000).
[4] N. Fang, H. Lee, C. Sun, and X. Zhang, Science **308**, 534 (2005).
[5] A. Giannattasio, I. R. Hooper, and W. L. Barnes, Opt. Express **12**, 5881 (2004).
[6] D. R. Smith, D. Schurig, M. Rosenbluth, S. Schultz, S. A. Ramakrishna, and J. B. Pendry, Appl. Phys. Lett. **82**, 1506 (2003).
[7] J. B. Pendry, L. Martín-Moreno, and F. J. Garcia-Vidal, Science **305**, 847 (2004).
[8] F. J. Garcia-Vidal, L. Martín-Moreno, and J. B. Pendry, Journal of Optics A: Pure and Applied Optics **7**, S97 (2005).
[9] E. Hendry, A. P. Hibbins, and J. R. Sambles, Phys. Rev. B **78**, 235426 (2008).
[10] F. García de Abajo and J. Sáenz, Phys. Rev. Lett. **95**, 233901 (2005).
[11] Y.-C. Lan and R.-L. Chern, Opt. Express **14**, 11339 (2006).
[12] L. Shen, X. Chen, and T.-J. Yang, Opt. Express **16**, 3326 (2008).
[13] S. A. Maier and S. R. Andrews, Appl. Phys. Lett. **88**, 251120 (2006).
[14] A. P. Hibbins, B. R. Evans, and J. R. Sambles, Science **308**, 670 (2005).
[15] A. P. Hibbins, E. Hendry, M. J. Lockyear, and J. R. Sambles, Opt. Express **16**, 20441 (2008).
[16] C. R. Williams, S. R. Andrews, S. A. Maier, A. I. Fernández-Domínguez, L. Martín-Moreno, and F. J. García-Vidal, Nature Photonics **2**, 175 (2008).
[17] R. Ulrich and M. Tacke, Appl. Phys. Lett. **22**, 251 (1973).
[18] T. Isaac, W. Barnes, and E. Hendry, Phys. Rev. B **80**, 115423 (2009).
[19] A. Hibbins, M. Lockyear, I. Hooper, and J. Sambles, Phys. Rev. Lett. **96**, 073904 (2006).
[20] L. Martín-Moreno, F. J. García-Vidal, H. J. Lezec, K. M. Pellerin, T. Thio, J. B. Pendry, and T. W. Ebbesen, Phys. Rev. Lett. **86**, 1114 (2001).
[21] J. Bravo-Abad, L. Martín-Moreno, F. García-Vidal, E. Hendry, and J. Gómez Rivas, Phys. Rev. B **76**, 241102 (2007).
[22] R. C. McPhedran, G. H. Derrick, and L. C. Botten, in *Electromagnetic Theory of Gratings*, edited by R. Petit (Springer-Verlag, Berlin, 1980).
[23] E. Kretschmann and H. Raether, Z. Naturforsch A **23**, 2135 (1968).
[24] I. Hooper and J. Sambles, Phys. Rev. B **70**, 045421 (2004).
[25] H. Raether, *Surface Plasmons* (Spring-Verlag, New York, 1986).
[26] Anritsu, vectorstar ms4644a.
[27] Hfss, high-frequency structure simulator version 13 finite-element package, Ansoft Corporation, Pittsburgh, PA, 2010.
[28] E. Economou, Phys. Rev. **182**, 539 (1969).
[29] J. Jung, F. García-Vidal, L. Martín-Moreno, and J. Pendry, Phys. Rev. B **79**, 153407 (2009).
[30] T. H. Isaac, Appl. Phys. Lett. **93**, 241115 (2008).
[31] M. de Dood, E. Driessen, D. Stolwijk, and M. van Exter, Phys. Rev. B **77**, 115437 (2008).
[32] H. Cao and A. Nahata, Opt. Express **12**, 1004 (2004).
[33] F. Miyamaru and M. Hangyo, Appl. Phys. Lett. **84**, 2742 (2004).
[34] J. F. O'Hara, R. D. Averitt, and A. J. Taylor, Opt. Express **12**, 6397 (2004).
[35] D. Qu, D. Grischkowsky, and W. Zhang, Opt. Lett. **29**, 896 (2004).
[36] E. Hendry, M. J. Lockyear, J. Gomez Rivas, L. Kuipers, and M. Bonn, Phys. Rev. B **75**, 235305 (2007).
[37] M. Beruete, M. Sorolla, I. Campillo, J. S. Dolado, L. Martín-Moreno, J. Bravo-Abad, and F. J. García-Vidal, Opt. Lett. **29**, 2500 (2004).
[38] H. Caglayan, I. Bulu, and E. Ozbay, Opt. Express **13**, 1666 (2005).
[39] H.-S. Lee, Y.-T. Yoon, S.-s. Lee, S.-H. Kim, and K.-D. Lee, Opt. Express **15**, 15457 (2007).
[40] A. Dhawan, M. D. Gerhold, and J. F. Muth, IEEE Sensors Journal **8**, 942 (2008).
[41] M. Beruete, M. Sorolla, I. Campillo, and J. Dolado, IEEE Microwave and Wireless Components Letters **15**, 116 (2005).
[42] C.-L. Pan, C.-F. Hsieh, R.-P. Pan, M. Tanaka, F. Miyamaru, M. Tani, and M. Hangyo, Opt. Express **13**, 3921 (2005).
[43] C. Genet, Opt. Commun. **225**, 331 (2003).
[44] W. L. Barnes, T. W. Preist, S. C. Kitson, and J. R. Sambles, Phys. Rev. B **54**, 6227 (1996).